Cluster observations of energetic electrons and electromagnetic fields within a reconnecting thin current sheet in the Earth's magnetotail

A. Retinò, R. Nakamura, A. Vaivads, Y. Khotyaintsev, T. Hayakawa, K. Tanaka, S. Kasahara, M. Fujimoto, I. Shinohara, J. P. Eastwood, et al.

▶ **To cite this version:**

A. Retinò, R. Nakamura, A. Vaivads, Y. Khotyaintsev, T. Hayakawa, et al.. Cluster observations of energetic electrons and electromagnetic fields within a reconnecting thin current sheet in the Earth's magnetotail. Journal of Geophysical Research Space Physics, 2008, 113 (A12), 10.1029/2008JA013511 . hal-04110229

HAL Id: hal-04110229
https://hal.science/hal-04110229

Submitted on 5 Jun 2023

HAL is a multi-disciplinary open access archive for the deposit and dissemination of scientific research documents, whether they are published or not. The documents may come from teaching and research institutions in France or abroad, or from public or private research centers.

L'archive ouverte pluridisciplinaire **HAL**, est destinée au dépôt et à la diffusion de documents scientifiques de niveau recherche, publiés ou non, émanant des établissements d'enseignement et de recherche français ou étrangers, des laboratoires publics ou privés.

Copyright

Cluster observations of energetic electrons and electromagnetic fields within a reconnecting thin current sheet in the Earth's magnetotail

A. Retinò,[1] R. Nakamura,[1] A. Vaivads,[2] Y. Khotyaintsev,[2] T. Hayakawa,[3] K. Tanaka,[4] S. Kasahara,[4] M. Fujimoto,[4] I. Shinohara,[4] J. P. Eastwood,[5] M. André,[2] W. Baumjohann,[1] P. W. Daly,[6] E. A. Kronberg,[6] and N. Cornilleau-Wehrlin[7]

Received 26 June 2008; revised 6 September 2008; accepted 30 September 2008; published 27 December 2008.

[1] We study the acceleration of energetic electrons during magnetotail reconnection by using Cluster simultaneous measurements of three-dimensional electron distribution functions, electric and magnetic fields, and waves in a thin current sheet. We present observations of two consecutive current sheet crossings where the flux of electrons 35–127 keV peaks within an interval of tailward flows. The first crossing shows the signatures of a tailward moving flux rope. The observed magnetic field and density indicate that the flux rope was very dynamic, and a comparison with numerical simulation suggests a crossing right after coalescence of smaller flux ropes. The second crossing occurs within the ion diffusion region. The flux of electrons is largest within the flux rope where they are mainly directed perpendicular to the magnetic field. At the magnetic separatrices, the fluxes are smaller, but the energy spectra are harder and electrons are mainly field aligned. Reconnection electric fields $E_Y \sim 7$ mV/m are observed within the diffusion region, whereas in the flux rope, E_Y are much smaller. Waves around lower hybrid frequency do not show a clear correlation with energetic electrons. We interpret the field-aligned electrons at the separatrices as directly accelerated by the reconnection electric field in the diffusion region, whereas we interpret the perpendicular electrons as trapped within the flux rope and accelerated by a combination of betatron acceleration with nonadiabatic pitch-angle scattering. Our observations indicate that thin current sheets during dynamic reconnection are important for in situ production of energetic electrons and that simultaneous measurements of electrons and electromagnetic fields within thin sheets are crucial to understand the acceleration mechanisms.

Citation: Retinò, A., et al. (2008), Cluster observations of energetic electrons and electromagnetic fields within a reconnecting thin current sheet in the Earth's magnetotail, *J. Geophys. Res.*, *113*, A12215, doi:10.1029/2008JA013511.

1. Introduction

[2] A key but yet poorly understood issue in astrophysical plasmas is the role of magnetic reconnection for the acceleration of energetic particles [*Sonnerup*, 1979; *Haerendel*, 1981]. Energetic particles are ions and electrons with energies much larger than their thermal energy ($\varepsilon \gg k_B$T). As an example, remote observations of solar flares indicate that a large fraction of energy is released as energetic electrons during magnetic reconnection [*Lin et al.*, 2003]. Many models and numerical simulations have been proposed to explain such energization (see, e.g., *Aschwanden* [2004] and references therein). However in situ observations are necessary to understand in detail the acceleration mechanisms during magnetic reconnection. The Earth's magnetotail is an excellent laboratory to study energetic electron acceleration during reconnection by using in situ spacecraft data. Pioneering observations in the magnetotail showed burst of energetic electrons ($\varepsilon \geq$ 200 keV) within the magnetotail plasma sheet and associated them with acceleration by magnetic reconnection in localized regions [*Baker and Stone*, 1976, 1977; *Richardson et al.*, 1996]. Those observations suggested that the strongest acceleration is most likely very localized in space and time. Later observations confirmed this interpretation by showing energetic electrons (ε up to $\sim$300 keV) accelerated within the ion diffusion region of reconnection [*Øieroset*

[1]Space Research Institute, Austrian Academy of Sciences, Graz, Austria.
[2]Swedish Institute of Space Physics, Uppsala, Sweden.
[3]Department of Earth and Planetary Sciences, Tokyo Institute of Technology, Meguro, Japan.
[4]Institute of Space and Astronautical Science, Japan Aerospace Exploration Agency, Sagamihara, Japan.
[5]Space Sciences Laboratory, University of California, Berkeley, California, USA.
[6]Max Planck Institute for Solar System Research, Katlenburg-Lindau, Germany.
[7]Centre d'Etude des Environnements Terrestre et Planétairs, CNRS/IPSL, Vélizy, France.

Copyright 2008 by the American Geophysical Union.
0148-0227/08/2008JA013511

et al., 2002]. Recent particle-in-cell simulations have addressed the microphysics of thin reconnecting current sheets to study whether energetic electrons are accelerated around the X-line directly by reconnection electric fields [*Pritchett*, 2006a, 2006b] or by other mechanisms such as acceleration at magnetic flux pile-up in the outflow region [*Hoshino et al.*, 2001] or Fermi acceleration in contracting small-scale magnetic islands [*Drake et al.*, 2006a]. Energetic electrons have been also predicted to be accelerated by lower hybrid waves produced within reconnection regions [*Cairns and McMillan*, 2005]. Recent Cluster observations have provided some evidence for these acceleration mechanisms. *Imada et al.* [2007] reported on energetic electrons in the magnetic flux pile-up region close to the X-line and found that the observations were consistent with the mechanism suggested by *Hoshino et al.* [2001]. *Chen et al.* [2008] reported evidence of energetic electrons within small-scale magnetic islands. *Åsnes et al.* [2008] reported on field-aligned energetic electron beams associated with tailward reconnection flows. *Asano et al.* [2008] discussed the relationship between lower energy (flat top) and energetic electron distribution functions during reconnection and suggested that the generation mechanisms of the two electron components were not directly related. However none of these observations reported simultaneously electric and magnetic fields and waves together with three-dimensional high-time resolution measurements of energetic electrons in reconnecting current sheets. These measurements are crucial for understanding the acceleration mechanisms of energetic electrons during magnetic reconnection. Here we present Cluster simultaneous observations of energetic electrons and electromagnetic fields in thin reconnecting current sheet and suggest possible acceleration mechanisms.

2. Event Overview

[3] We present Cluster multispacecraft observations in the Earth's magnetotail on 24 August 2003. The event was previously studied by *Nakamura et al.* [2006] who analyzed the properties of several thin current sheets associated with reconnection. Cluster was located at (−17, −4,3) R_E GSM with a maximum spacecraft separation of ∼200 km [*Nakamura et al.*, 2006, Figure 1]. We use data from several instruments onboard Cluster: (1) magnetic field **B** from FGM [*Balogh et al.*, 2001], (2) electric field **E** and probe-to-spacecraft potential from EFW [*Gustafsson et al.*, 2001], (3) electric and magnetic wave spectrograms from STAFF [*Cornilleau-Wehrlin et al.*, 1997], (4) ion differential energy flux *dEF* and velocity **V** from CIS/CODIF [*Réme et al.*, 2001], (5) electron differential energy flux *dEF* from PEACE [*Johnstone et al.*, 1997], (6) energetic electron differential flux *dF* from RAPID/IES [*Wilken et al.*, 2001]. The plasma density N is obtained from the probe-to-spacecraft potential [*Pedersen et al.*, 2001].

[4] Figure 1 shows an overview of the event for SC/4. In the time interval 1830–1834 UT Cluster is in the plasma sheet proper observing hot ∼ 1 keV electrons, Figure 1d, and ∼ 10 keV ions, Figure 1e. From 1834 Cluster observe a thinning of the current sheet, as indicated by the increase of B_X, Figure 1a, and discussed in detail by *Nakamura et al.* [2006]. Around 1840 SC/4 crosses the current sheet from the northern to southern hemisphere. In the time interval 1840–1846 the spacecraft observe tailward flows, Figure 1b, at approximately Alfvén speed V_A = 985 km/s (calculated from $B_{\rm lobe}$ = 20 nT and N_{lobe} = 0.2 cm^{-3}). Finally 1846–1850 SC/4 exits the plasma sheet to enter the southern lobe/plasma sheet boundary layer where no fast flows are detected.

[5] Figures 1c to 1e show the acceleration and heating of ions and electrons during the fast flows. In particular Figure 1c clearly shows enhancements of the differential flux *dF* of energetic electrons within the interval of fast flows with respect to both the plasma sheet proper 1830–1834 and the lobe/plasma sheet boundary layer 1846–1850. We note however that a one-to-one correlation between *dF* and the flow velocity is not clearly observed. We also note that *dF* does not just increase when Cluster cross the current sheet, e.g., around 1842 $B_X \sim 0$ and d*F* is very small. This indicates that energetic electrons are not always enhanced in the center of the current sheet. Energetic electrons are also found in a later interval 1905–1920 where earthward flows are observed (not shown). The flux of energetic electrons during earthward flows is much larger than during tailward flows, as already reported by *Imada et al.* [2005] and *Åsnes et al.* [2008]. The detailed analysis of the energetic electrons in the earthward flow region is ongoing and it will be presented elsewhere.

[6] In this paper we focus on the two current sheet crossings around 184300, shaded yellow in Figure 1a, since the highest *dF* of energetic electrons are observed there within the interval of tailward fast flows, Figure 1c. A zoom-in of these two current sheet crossings is shown in Figure 2, where we present data for SC/2 since this is the only spacecraft for which three-dimensional measurements of *dF* (8 energies, 9 polar angles, 16 azimuthal angles) are available from RAPID/IES. These measurements are required to resolve the pitch-angle distributions of energetic electrons, as it is discussed in section 4.

3. Properties of the Thin Current Sheet

[7] Figures 3b–3d present four-point magnetic field observations during the first current sheet crossing 184304–184312 shown in Figure 2. The observations show signatures of a tailward moving flux rope, namely a ± normal magnetic field B_Z and an increase of the out-of-plane magnetic field B_Y at the center of the current sheet. Combined timing and minimum variance analysis on the magnetic field for SC/1–4 give the local current sheet coordinate system **L** = (0.95;0.16; −0.25), **M** = (−0.13;0.95;0.14), **N** = (0.04; −0.14; 0.99) GSM. The LMN system is very close to GSM (also for the second current sheet crossing) thus vectors are shown everywhere in GSM. Using the time delays among spacecraft we estimate a current sheet velocity $V_{cs} \sim$ 250 km/s in the normal direction **N** to the sheet plane and a current sheet thickness $\sim 4\lambda_i \sim$ 2000 km where λ_i = 510 km is the ion inertial length. Figures 3b–3e show that the spacecraft observe approximately the same magnetic field and density thus indicating that the current sheet is approximately planar over the spacecraft separation ∼200 km and that the flux rope is more elongated in X than in Z. This is consistent with a flux rope velocity ∼850 km/s in the X direction and a flux rope aspect ratio ∼3 between the X and Z directions

21562202a, 2008, A12, Downloaded from https://agupubs.onlinelibrary.wiley.com/doi/10.1029/2008JA013511 by Cochrane France, Wiley Online Library on [04/06/2023]. See the Terms and Conditions (https://onlinelibrary.wiley.com/terms-and-conditions) on Wiley Online Library for rules of use; OA articles are governed by the applicable Creative Commons License

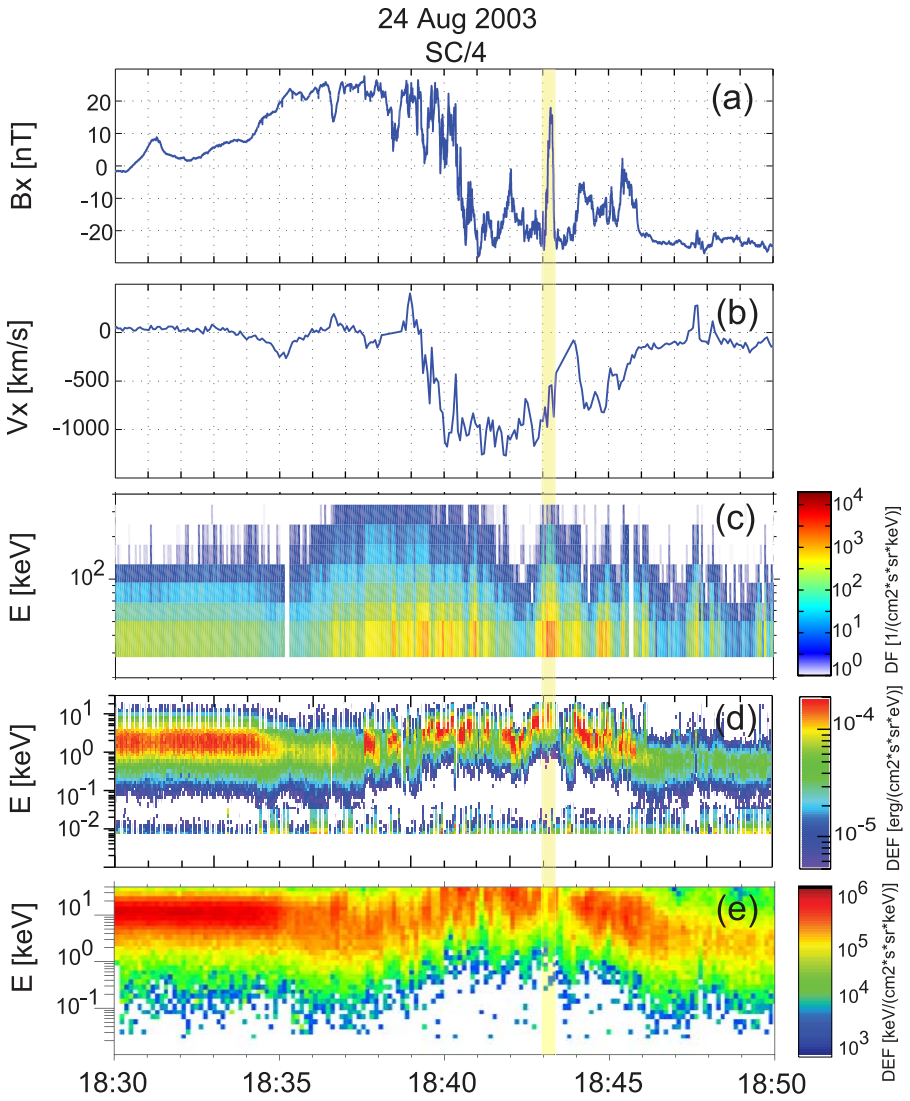

Figure 1. (a) B_x from FGM sampled at 22 Hz, (b) V_x from CIS/CODIF, (c) RAPID/IES differential flux *dF* spectrogram in the range 28-336.5 keV, (d) combined PEACE/HEEA and PEACE/LEEA differential energy flux *dEF* spectrogram in the range 10 eV-26.5 keV, and (e) CIS/CODIF *dEF* spectrogram in the range 20 eV-40 keV. RAPID, PEACE and CIS data have 4s time resolution. Vectors are in GSM. The current sheet crossings are shaded yellow.

estimated by *Nakamura et al.* [2006]. The change in B_X, Figure 3b, occurs in two major steps indicating current sheet bifurcation. There is a guide field of ~10 nT, Figure 3c (~50% of the reconnecting component B_X). B_Y increases by a factor two over the guide field in the center of the current sheet while simultaneously B_Z, Figure 3d, shows the ± perturbation. The density, Figure 3e, shows a large increase within the current sheet simultaneous to the B_Y increase. All the observed features indicate that the spacecraft crossed a flux rope propagating in tailward direction, as expected for the tailward reconnection jets observed in this event. The observed features are consistent with earlier observations of flux ropes [*Slavin et al.*, 2003; *Eastwood et al.*, 2007; *Chen et al.*, 2008] and have been found in numerical simulations of guide field reconnection [*Drake et al.*, 2006b; *Pritchett*, 2006b].

[8] A closer inspection of the magnetic field and density profiles reveals that the flux rope was rather structured at the time of Cluster crossing. There is a clear asymmetry between the leading and trailing edges of the flux rope, the changes in magnetic field and density being sharper at the leading edge. A key feature is the density dip in the center of the flux rope that is revealed by the high-time resolution measurement of the density from EFW spacecraft potential and is observed at the same time when B_Y is maximum. This feature suggests a more complicated dynamics within the flux rope than a simple compression of plasma and magnetic field.

[9] To facilitate the interpretation of the flux rope structure and dynamics, we made a comparison with a two-dimensional full particle numerical simulation [*Tanaka et al.*, 2004]. The initial magnetic field is one Harris current sheet $B_x(z) = B_{lobe}\tanh(z/D)$ including an uniform guide

21562202a, 2008, A12, Downloaded from https://agupubs.onlinelibrary.wiley.com/doi/10.1029/2008JA013511 by Cochrane France, Wiley Online Library on [04/06/2023]. See the Terms and Conditions (https://onlinelibrary.wiley.com/terms-and-conditions) on Wiley Online Library for rules of use; OA articles are governed by the applicable Creative Commons License

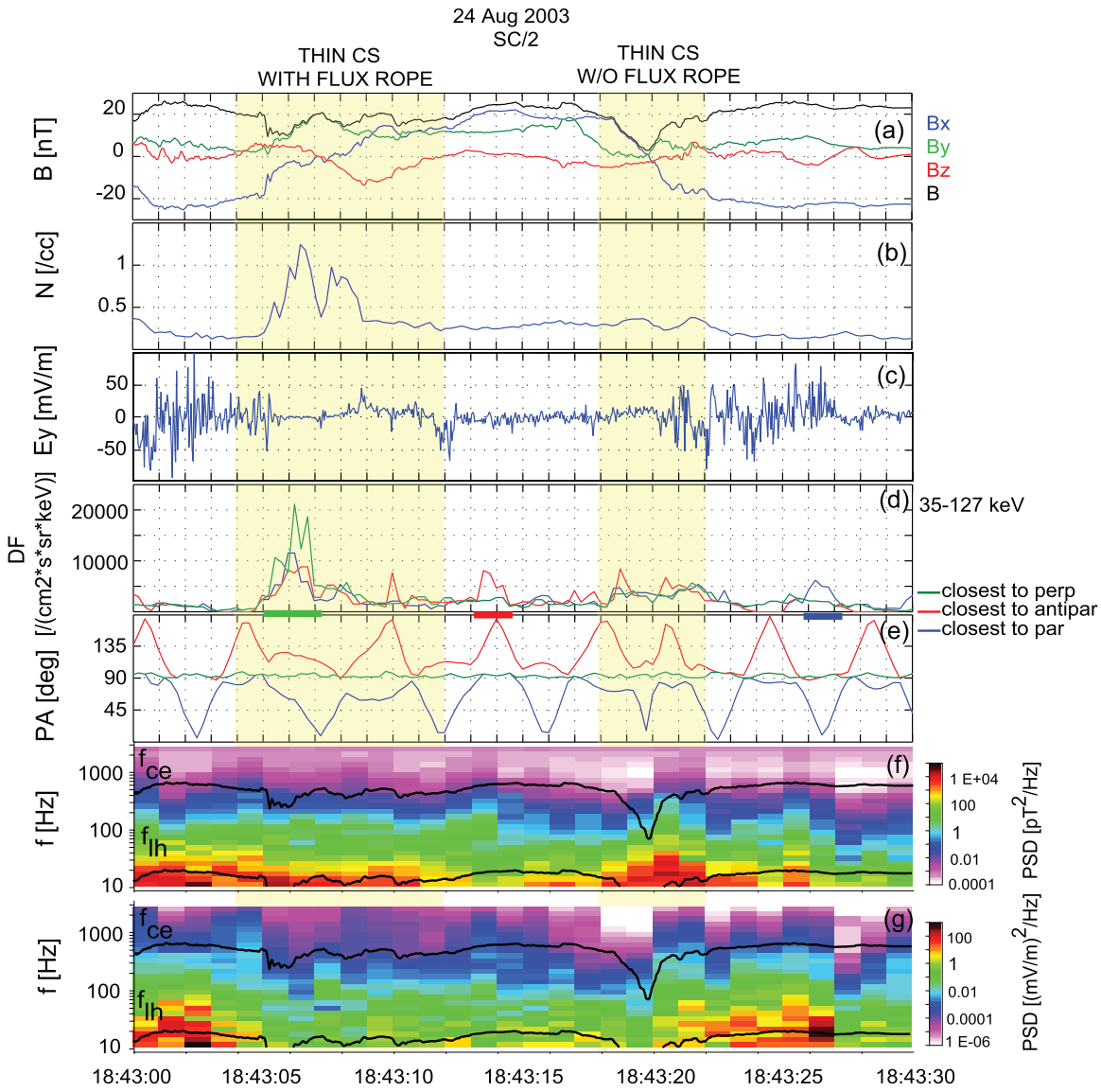

Figure 2. (a) **B**; (b) N sampled at 5 Hz; (c) E_Y sampled at 25 Hz in the range 0–180 Hz; and (d) dF in the energy range 35–127 keV measured at directions closest to perpendicular (green), antiparallel (red), and parallel (blue) with time resolution of 0.25 s. Horizontal bars indicate averaging intervals for $f(\varepsilon)$ shown in Figure 4; (e) pitch-angle of the directions closest to 90° (green), 180° (red), and 0° (blue); (f) magnetic field wave spectrogram measured by STAFF with time resolution of 1 s in the range 8 Hz–4 kHz, and (g) electric field wave spectrogram measured by STAFF with time resolution of 1 s in the range 8 Hz–4 kHz. Solid lines in Figures 2f–2g show the electron gyrofrequency f_{ce} and the lower hybrid frequency f_{lh}. All vectors are in GSM. The current sheets crossings are shaded yellow.

field $B_{y0} = 0.5\ B_{lobe}$, where B_{lobe} is the magnitude of the lobe field and D is the half thickness of the current sheet. Plasma sheet density N_{ps} and B_{lobe} are the units for N and **B** and the ion-to-electron temperature ratio is $T_{i,ps}/T_{e,ps} = 8$. Temporal and spatial scales are normalized to λ_i and to the inverse of the ion gyrofrequency Ω_i^{-1} respectively, while the velocity is normalized to the Alfvén velocity V_A. The ion-to-electron mass ratio is $m_i/m_e = 25$ and $D = 0.5$. The dimensions of the simulation box are $(-L_x/2;\ L_x/2) \times (-L_z/2;\ L_z/2)$ in normalized units with $L_x = L_z$. Periodic boundary conditions are imposed in X while conducting walls are set at the Z boundary. Reconnection is triggered by GEM initial perturbation [*Birn and Hesse*, 2001]. The number of the perturbations along X corresponds to the number of initial flux ropes n_{fr}. The system length is $L_x = n_{fr}\lambda_{\max}$ with $\lambda_{\max} = 12D$ fastest growing mode of the tearing mode [*Brittnacher et al.*, 1995].

[10] We have chosen as best agreement between observations and simulation the case when a density dip and maximum B_Y are simultaneously found in the center of the flux rope. A parametric survey of the initial number of flux ropes n_{fr} gives $n_{fr} = 4$ as best agreement with the observations. Starting with $n_{fr} = 4$, the system reduces first to two flux ropes and then to one flux rope through coalescence. At

21562202a, 2008, A12, Downloaded from https://agupubs.onlinelibrary.wiley.com/doi/10.1029/2008JA013511 by Cochrane France, Wiley Online Library on [04/06/2023]. See the Terms and Conditions (https://onlinelibrary.wiley.com/terms-and-conditions) on Wiley Online Library for rules of use; OA articles are governed by the applicable Creative Commons License

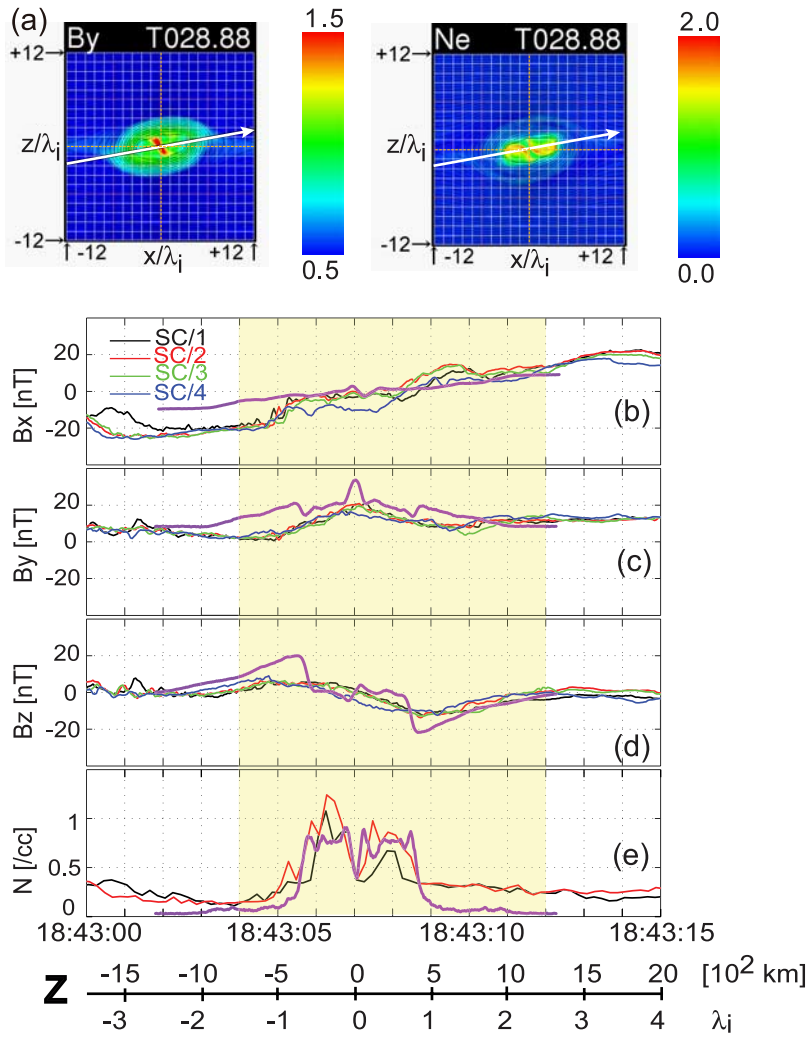

Figure 3. (a) Two-dimensional snapshots of normalized B_Y and N (color coded) from the simulation run in the XZ GSM plane. Normalization units are B_{lobe} and plasma sheet density N_{ps}. The arrows represent the virtual spacecraft trajectory. The angle between X axis and virtual trajectory is 10°, (b) B_X, (c) B_Y, (d) B_Z, and (e) N. N is not available for SC/3 and SC/4 since ASPOC was active. Vectors are in GSM. **B** and N are time shifted using time delays among spacecraft. The current sheet crossing is shaded yellow. Violet lines in panels 3b to 3e show the simulation values along the virtual spacecraft trajectory. For the comparison, B_{lobe} = 20 nT and N_{ps} = 0.5 cm^{-3} are set for the simulation. The spatial scale bar on the bottom shows the spacecraft position in Z direction (with respect to the center of the current sheet $Z = 0$) in kilometers unit and in lobe ion inertial length unit (λ_i = 510 km).

t = 28.88 during the simulation run with n_{fr} = 4, B_Y and N, color coded in Figure 3a, show simultaneously a density dip and maximum B_Y in the center of the flux rope. The time t = 28.8 is right after the coalescence of two flux ropes into a larger one (occurring at t = 25). Figures 3b to 3e show the simulation values of B_X, B_Y, B_Z and N (violet lines) along the virtual spacecraft trajectory plotted over Cluster measurements. The simulation shows a reasonable agreement with the observations. Both the enhancement of density within the island and the dip of density at the center are well reproduced. The increase in B_Y within the island is also reproduced though the simulation value at the center is larger. The largest differences are observed in B_X and B_Z. This can be explained by the fact that the flux rope in the observations is more elongated in the X direction compared to the simulation. The simulation also confirms that the flux rope has a typical scale of a few ion inertial lengths. The comparison between observations and simulation suggests that Cluster might have crossed the flux rope right after coalescence of smaller flux ropes at times when the flux rope was very structured and dynamic.

[11] The second current sheet crossing 184318–184322 has been studied earlier by *Nakamura et al.* [2006]. They presented detailed current estimations and electron distribution function observations (in the energy range 1.5–5 keV) to show that the current sheet thickness was of the order of $\sim\lambda_i$ and that Cluster crossed the current sheet in the ion diffusion region of reconnection with no guide field. In particular, Figure 5 of *Nakamura et al.* [2006] shows field-aligned 1.5–5 keV electrons on the two sides of the current

21562202a, 2008, A12, Downloaded from https://agupubs.onlinelibrary.wiley.com/doi/10.1029/2008JA013511 by Cochrane France, Wiley Online Library on [04/06/2023]. See the Terms and Conditions (https://onlinelibrary.wiley.com/terms-and-conditions) on Wiley Online Library for rules of use; OA articles are governed by the applicable Creative Commons License

sheet streaming antiparallel, parallel to the magnetic field around 184315, 184325 respectively. These electrons are accelerated away from the X-line on both sides of the diffusion region and are associated with the Hall current system in the separatrix region of reconnection.

4. Observations of Energetic Electrons, Fields, and Waves

[12] We now present detailed observations of energetic electrons, electric and magnetic fields and waves for the two current sheet crossings discussed in the previous section. We use high-time resolution measurements of differential flux *dF* from RAPID/IES where *dF* is measured every 0.25 s. This time interval corresponds to one azimuthal sector in the spacecraft spin plane, as discussed by *Imada et al.* [2007]. We obtain the pitch-angle *dF* by projecting the instantaneous magnetic field into the 9 polar sectors of the detector.

[13] Figure 2d shows *dF* in the energy range 35–127 keV at pitch-angles which are, at each time, the closest to perpendicular (green), antiparallel (red) and parallel (blue) directions. It should be noted that, because of relative orientation between the RAPID/IES detector and the magnetic field, not all the pitch-angles can be simultaneously measured at each time as discussed by *Wilken et al.* [2001]. Figure 2e shows the actual pitch-angles of the directions closest to perpendicular, parallel and antiparallel. The perpendicular direction is always measured while parallel and antiparallel directions are measured approximately once every spacecraft spin (~4 s). The directions closest to 0°, 180° are often within 45°–90°, 90°–135° respectively. The high-time resolution and pitch-angle information allow to reveal the details of the energetic electrons within the current sheet crossings.

[14] The largest *dF* is observed within the flux rope in the time interval 184305–184307.2, green horizontal bar in Figure 2d, which corresponds to the leading edge of the flux rope. In this time interval the *dF* at ~90° with respect to the local magnetic field direction is larger than at the directions closest to ~0° and ~180°. It should be noted that the ~90° and ~0°, ~180° directions are not simultaneously measured during this interval. Nevertheless the *dF* at ~90° right after 184307, when both ~0° and ~90° directions are simultaneously measured, is still a factor two larger than the d*F* at ~0°. The *dF* on the trailing edge of the flux rope is smaller than on the leading edge and more isotropic in pitch angle. The largest *dF* enhancement within the flux rope is not correlated with strong waves either in the lower hybrid frequency range f_{lh} or in the electron gyrofrequency range f_{ce}, Figure 2. The DC electric field where the d*F* is largest is also rather weak (~ few mV/m), Figure 2c.

[15] The *dF* has other major enhancements within and around the diffusion region, corresponding to the second current sheet crossing 184318–184322. Two major enhancements are observed on the sides of the current sheet. In the time interval 184312–184318, the electrons are mainly directed antiparallel to the magnetic field. The *dF* at ~180° is in fact dominant when ~90°, ~180° directions are simultaneously measured (184313.2–184314.5, red horizontal bar) while when ~0°, ~90° directions are measured the *dF* is smaller and more isotropic. The opposite happens 184322–184330 when the electrons are mainly directed parallel to the magnetic field. The *dF* in this case is dominant when ~0°, ~90° are simultaneously measured (184325.8–184327.3, blue horizontal bar). It should be noted that in both cases the electrons are streaming away from the diffusion region i.e., in tailward direction. The second enhancement of the *dF*, blue horizontal bar, is correlated with strong waves around the lower hybrid frequency which are observed both by EFW, Figure 2c, and by STAFF, Figures 2f–2g. However lower hybrid waves are not observed at the first enhancement of the *dF*, red bar. No strong waves around f_{ce} are observed in both cases. The DC electric field at the first enhancement of the *dF*, red bar, is weak while at the second enhancement, blue bar, is difficult to determine since it is dominated by the lower hybrid waves (EFW is measuring in the frequency range 0–180 Hz which contains f_{lh}). Within the diffusion region the *dF* of energetic electrons is mostly isotropic. In particular in the center of the current sheet 184320, where the total magnetic field is smallest, both ~0° and ~90° directions are approximately simultaneously measured and the *dF* in both directions are equal. Waves around the lower hybrid range are observed within the current sheet but mainly at the edges. The DC electric field around the center of the current sheet is large E_Y ~7 mV/m (averaged on the time interval 184318.5–184320 where no waves were observed).

[16] Figure 4 shows the phase space density $f(\varepsilon)$ for three major enhancements of the energetic electrons observed during the current sheet crossings. The phase space density $f(\varepsilon)$ is obtained from the measured differential flux $dF(\varepsilon)$ by using the relationship $f(\varepsilon) = \frac{m_e^2}{2\varepsilon} dF(\varepsilon)$, where m_e is the electron mass [*Baumjohann and Treumann*, 1996]. The green line in the figure represents $f(\varepsilon)$ measured at ~90° and averaged over the time interval 184305–184307.2 within the flux rope (green horizontal bar in Figure 2). The red line represents $f(\varepsilon)$ measured at ~180° and averaged in time over 184313.2–184314.5 around one separatrix (red horizontal bar in Figure 2). The blue line represents $f(\varepsilon)$ measured at ~0° and averaged in time over 184325.8–184327.3 around the other separatrix (blue horizontal bar in Figure 2). The dashed lines in Figure 4 are power law $\varepsilon^{-\gamma}$ fits to the measured $f(\varepsilon)$ and are shown together with the best fit values of the spectral index γ. The figure shows that the energy spectra for the field-aligned electrons on both sides of the diffusion region are harder (γ = 3.9) than the spectrum of perpendicular electrons within the flux rope (γ = 5.6). The values of γ are not much sensitive to the choice of the averaging interval for $f(\varepsilon)$ as the fits done at instantaneous peak values of $f(\varepsilon)$ give approximately the same γ. The values of the spectral indexes when the fit is done on *dF* are 2.9 for ~0°,180° and 4.6 for ~90°.

5. Discussion

[17] Our observations show, at least for this particular event, that energetic electrons are anisotropic with respect to the magnetic field direction and that they have different pitch-angle distributions at different locations within and around the thin current sheet. Earlier observations by *Chen et al.* [2008] established the importance of small-scale flux ropes for the acceleration of energetic electrons but the

21562202a, 2008, A12, Downloaded from https://agupubs.onlinelibrary.wiley.com/doi/10.1029/2008JA013511 by Cochrane France, Wiley Online Library on [04/06/2023]. See the Terms and Conditions (https://onlinelibrary.wiley.com/terms-and-conditions) on Wiley Online Library for rules of use; OA articles are governed by the applicable Creative Commons License

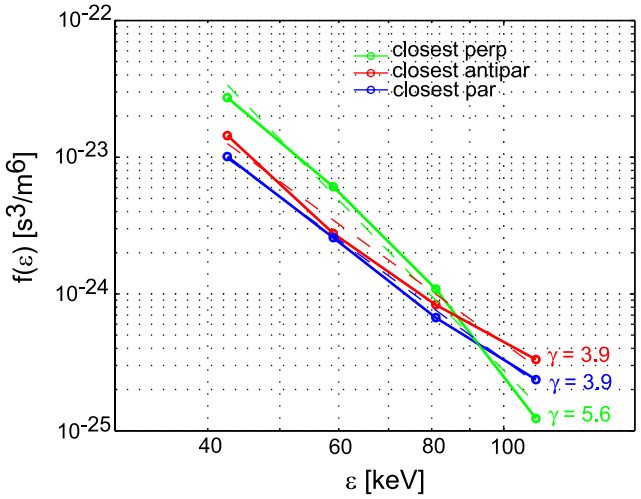

Figure 4. Phase space density $f(\varepsilon)$ at the three enhancements indicated by horizontal bars in Figure 2: closest to 90° averaged over 184305–184307.2 (green), closest to 180° averaged over 184313.2–184314.5 (red), and closest to 0° averaged over 184325.8–184327.3 (blue). Dashed lines are best fit to power laws $\varepsilon^{-\gamma}$.

pitch-angle distributions of electrons were not discussed since no three-dimensional distribution functions were available. Our observations of perpendicular electrons within the small-scale flux rope indicate that pitch-angle distribution functions are important to study the acceleration of energetic electrons within small-scale flux ropes. Our observations of field-aligned electrons on both sides of the diffusion region are in agreement with observations by *Åsnes et al.* [2008], who recently reported on a near-Earth reconnection event with field-aligned energetic electrons (up to ~127 keV) streaming away from the diffusion region within tailward flows. Our observations of isotropic energetic electrons in the diffusion region are in agreement with those of *Øieroset et al.* [2002] who showed isotropic energetic electrons in the diffusion region above 6 keV.

[18] Our observations also show that energetic electrons have different energy spectra at different locations within and around the current sheet. The value $\gamma = 3.9$ found for $f(\varepsilon)$ on both sides of the diffusion region is similar to the values reported in observations around the diffusion region (4.8) [*Øieroset et al.*, 2002] and in the magnetic flux pile-up region close to the X-line (5.0) [*Imada et al.*, 2007] as well as in numerical simulations of driven reconnection (4.6) [*Pritchett*, 2006a]. The observed value $\gamma = 5.6$ within the flux rope is larger than all the above values.

[19] The differences in pitch-angles and energy spectra indicate that the energetic electrons have been accelerated by different mechanisms within and around the thin current sheet and/or that additional processes such as pitch-angle scattering by waves were operating in some cases.

[20] The field-aligned electrons on both sides of the diffusion region (red and blue bars) are streaming away from the X-line and are most likely observed around magnetic separatrices, as sketched in Figure 5. This is consistent with the observation at approximately same times of field-aligned 1.5–5 keV electrons accelerated away from the X-line and associated with Hall current system in the separatrix region (as shown in Figure 5 of *Nakamura et al.* [2006]). Furthermore the energetic electrons are observed where the density, Figure 2b, is slightly higher than in the lobe, also consistent with being in the separatrix region. We suggest that the field-aligned energetic electrons have been accelerated by the reconnection electric field E_Y within the diffusion region and observed by Cluster around magnetic separatrices. The observed pitch angles and energy spectra (power-law index $\gamma = 3.9$) are consistent with those found in a numerical simulation of driven reconnection without guide field by *Pritchett* [2006a] where electrons are accelerated in the vicinity of the X-line by the inductive electric field. The reconnection electric field observed by Cluster within the diffusion region (averaged on the time interval 184318.5–184320) is $E_Y \sim 7$ mV/m, Figure 2c. An electron accelerated in the out-of-plane direction by such electric field would gain ~127 keV over a distance $\sim 18 \cdot 10^3$km ~ $2.8R_E \sim 35\lambda_i$. Though we do not know the east-west extension of the current sheet, we note that the estimated acceleration distance is much smaller than the east-west extension of the magnetotail. By taking $B_{lobe} = 20$ nT and $V_A = 985$ km/s, we estimate a reconnection rate ~0.35 for the observed $E_Y \sim 7$ mV/m. This value of the reconnection rate is consistent with peak values of reconnection rate reported in the simulation by *Pritchett* [2006a]. The fact that the reconnection rate was much higher than the one expected for the steady state case (~0.1) indicates that Cluster crossed the current sheet when reconnection was unsteady (possibly close to reconnection onset). Our interpretation of energetic electrons directly accelerated by the reconnection electric field during unsteady reconnection is consistent with an earlier study by *Åsnes et al.* [2008]. In that study field-aligned energetic electrons were observed close to the diffusion region simultaneously by all Cluster spacecraft which were at larger separation than in our case (~ thousands km). The acceleration of energetic field-aligned electrons by lower hybrid waves, which has been suggested by *Cairns and McMillan* [2005], seems less consistent with our observations. Strong waves in the lower hybrid frequency range are observed around one separatrix together with an enhancement of the electron flux (blue horizontal bar in Figure 2d). However no waves are observed around the other separatrix (red bar) and no energetic electrons are found in the lobe 184300–184304 where strong lower hybrid waves were observed. Thus it is unclear from our observations if lower hybrid waves within

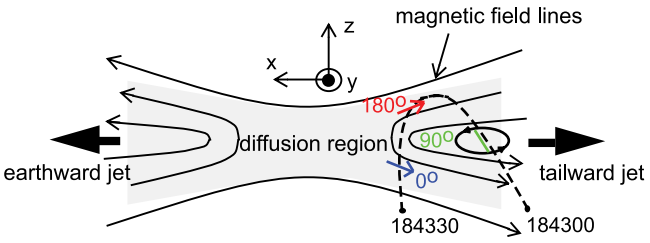

Figure 5. Cartoon of the current sheet crossings showing the locations and directions of energetic electrons. Cluster trajectory is dashed.

21562302a, 2008, A12, Downloaded from https://agupubs.onlinelibrary.wiley.com/doi/10.1029/2008JA013511 by Cochrane France, Wiley Online Library on [04/06/2023]. See the Terms and Conditions (https://onlinelibrary.wiley.com/terms-and-conditions) on Wiley Online Library for rules of use; OA articles are governed by the applicable Creative Commons License

and around thin current sheets are important for the acceleration of electrons in the energy range 35–127 keV.

[21] Within the small-scale flux rope, the highest fluxes of energetic electrons are observed in the direction perpendicular to the magnetic field. Figure 2d shows that, when the highest fluxes are observed (green horizontal bar), the perpendicular *dF* often increases when the total magnetic field *B* increases. However a one-to-one correlation is difficult to establish since the time resolution of *dF* (0.25 s) is much lower than the resolution of magnetic field measurements (0.045 s). A possibility is that electrons are trapped in the flux rope and are locally accelerated in perpendicular direction by drifting, on average, more into regions of stronger magnetic field than into regions of weaker field. The gyroradius of electrons with ε = 127 keV in the minimum magnetic field within the flux rope B = 10 nT is $\rho_{ce} \sim$ 130 km. Thus the gyroradius of the most energetic electrons is much smaller than the estimated size of the flux rope $\sim$ a few thousands km, consistent with the trapping condition. The time scale of the magnetic field variations within the flux rope $T_B \sim 0.1$ s is much larger than the electron gyroperiod $T_{ce} \sim 0.004$ s (computed for B = 10 nT), consistent with betatron adiabatic acceleration [*Baumjohann and Treumann*, 1996]. However it should be noted that lower hybrid waves, which are observed within the flux rope though with small amplitude (Figures 2f–2g), and/or spatial inhomogeneities within the flux rope could in principle scatter electrons and violate the conservation of the magnetic moment. This suggests that the actual acceleration mechanism for the trapped electrons within the flux rope is more some kind of gyrorelaxation/magnetic pumping (combination of betatron acceleration with nonadiabatic processes such as pitch-angle scattering) [*Alfvén and Fälthammar*, 1963] rather than adiabatic betatron acceleration. The largest relative variations of the total magnetic field within the flux rope are $\frac{\delta B}{B} \sim 1$. Since the typical energy gain during betatron acceleration is $\sim\frac{\delta B}{B}$ and during gyrorelaxation/magnetic pumping is $\sim (\frac{\delta B}{B})^2$, to get the observed energies $\sim$100 keV from $\sim$keV plasma sheet electrons the particles must have undergone such acceleration mechanisms multiple times. While we cannot exclude this possibility, we think that a more likely scenario is a two-step acceleration during which the electrons are first accelerated around the X-line by the reconnection electric field and then further accelerated within the flux rope, as discussed by *Scholer* [1984]. This would be consistent with the observation of the diffusion region at the second current sheet crossing a few ion gyroperiods later, as sketched in Figure 5. Furthermore the comparison with the numerical simulation in section 3 suggests that Cluster might have crossed the flux rope right after coalescence of smaller flux ropes and thus the electrons could have been accelerated by reconnection electric fields at more than one X-line. Observations of trapped energetic electrons within a plasmoid have been reported by *Zong et al.* [2004] though at larger spatial scales. Direct acceleration by a DC electric field and/or by lower hybrid waves within the flux rope seems unlikely since both the DC field and the waves were rather weak when the highest fluxes of electrons were observed. It should be also noted that the highest flux of energetic electrons within the flux rope coincides with a density enhancement. This correlation was established earlier by *Chen et al.* [2008] who suggested that the dominant acceleration mechanism within the flux rope and the density compression are strongly related. They however noted that the strongest density compressions do not always correspond to the highest electron fluxes, indicating that energetic electrons are not just produced by compression of background electrons. This is consistent with our observation at another density compression within the flux rope where the flux of electrons did not show a large enhancement.

6. Conclusions

[22] We have studied the acceleration of energetic electrons up to $\sim$100 keV during magnetic reconnection by using Cluster simultaneous measurements of three-dimensional high-time resolution electron distribution functions, DC electric fields and waves within two consecutive crossings of a thin current sheet in the Earth's magnetotail. The current sheet has the size of a few ion inertial lengths. This kind of measurements are crucial to study and understand in detail the acceleration mechanisms of energetic electrons during reconnection. The main conclusions obtained in this study can be summarized as follows:

[23] 1. Thin current sheets associated with dynamic reconnection are important for in situ production of energetic electrons.

[24] 2. Energetic electrons within the thin reconnecting current sheet are anisotropic with respect to the magnetic field direction and follow different power law spectra at different locations. The hardest spectrum is observed for field-aligned electrons at magnetic separatrices. The highest flux is observed within a small-scale flux rope for perpendicular electrons. Electrons within the flux rope have a softer spectrum than at separatrices.

[25] 3. Field-aligned electrons observed at magnetic separatrices are interpreted as directly accelerated by the reconnection electric field E_Y in the diffusion region during an interval of unsteady reconnection.

[26] 4. Perpendicular electrons observed in the small-scale flux rope are interpreted as produced by a two-step acceleration mechanism. Electrons are first accelerated in the diffusion region by the reconnection electric field and then trapped in the flux rope, where they are further accelerated by a combination of betatron acceleration with nonadiabatic pitch-angle scattering.

[27] 5. Waves in the lower hybrid frequency range do not show a clear correlation with energetic electrons.

[28] The results presented here have been obtained for a particular reconnection configuration. To improve our understanding of the acceleration mechanisms of energetic electrons, we will analyze in the future more simultaneous measurements of electron distribution functions, electric fields and waves within thin current sheets in different configurations such as steady/unsteady reconnection, different guide fields and different locations with respect to the X-line.

[29] In situ observations in the Earth's magnetotail like those reported here could be important to understand the acceleration of energetic electrons during reconnection in other space environments, e.g., in the solar corona where only remote observations are available. It is interesting to notice that the spectral index 2.9 observed at magnetic

21562202a, 2008, A12, Downloaded from https://agupubs.onlinelibrary.wiley.com/doi/10.1029/2008JA013511 by Cochrane France, Wiley Online Library on [04/06/2023]. See the Terms and Conditions (https://onlinelibrary.wiley.com/terms-and-conditions) on Wiley Online Library for rules of use; OA articles are governed by the applicable Creative Commons License

separatrices for the differential flux of electrons in the energy range ~30–100 keV is close to the index found in the same energy range by *Lin et al.* [2003] during the impulsive phase of a very intense solar flare. More comparisons between in situ and remotely measured energetic electrons spectra during reconnection will be done in future to confirm this approach.

[30] **Acknowledgments.** We acknowledge the CIS and PEACE teams for providing ion and electron data. Discussion with M. Taylor is acknowledged.

[31] Amitava Bhattacharjee thanks the reviewers for their assistance in evaluating this paper.

References

Alfvén, H., and C. G. Fälthammar (1963), *Cosmical Electrodynamics: Fundamental Principles*, Clarendon, Oxford, U.K.

Asano, Y., et al. (2008), Electron flat-top distributions around the magnetic reconnection region, *J. Geophys. Res.*, *113*, A01207, doi:10.1029/2007JA012461.

Aschwanden, M. J. (2004), *Physics of the Solar Corona: An Introduction*, Springer, New York.

Åsnes, A., M. G. G. T. Taylor, A. L. Borg, B. Lavraud, R. W. H. Friedel, C. P. Escoubet, H. Laakso, P. Daly, and A. N. Fazakerley (2008), Multi-spacecraft observation of electron beam in reconnection region, *J. Geophys. Res.*, *113*, A07S30, doi:10.1029/2007JA012770.

Baker, D. N., and E. C. Stone (1976), Energetic electron anisotropies in the magnetotail: Identification of open and closed field lines, *Geophys. Res. Lett.*, *3*, 557–560.

Baker, D. N., and E. C. Stone (1977), Observations of energetic electrons/E no less than about 200 keV/in the Earth's magnetotail: Plasma sheet and fireball observations, *J. Geophys. Res.*, *82*, 1532–1546.

Balogh, A., et al. (2001), The cluster magnetic field investigation: Overview of in-flight performance and initial results, *Ann. Geophys.*, *19*, 1207–1217.

Baumjohann, W., and R. A. Treumann (1996), *Basic Space Plasma Physics*, Imperial College Press, London, U.K.

Birn, J., and M. Hesse (2001), Geospace Environment Modeling (GEM) magnetic reconnection challenge: Resistive tearing, anisotropic pressure and Hall effects, *J. Geophys. Res.*, *106*, 3737–3750.

Brittnacher, M., K. B. Quest, and H. Karimabadi (1995), A new approach to the linear theory of single-species tearing in two-dimensional quasi-neutral sheets, *J. Geophys. Res.*, *100*, 3551–3562.

Cairns, I. H., and B. F. McMillan (2005), Electron acceleration by lower hybrid waves in magnetic reconnection regions, *Phys. Plasmas*, *12*, 102110, doi:10.1063/1.2080567.

Chen, L.-J., et al. (2008), Observation of energetic electrons within magnetic islands, *Nature Phys.*, *4*, 19–23, doi:10.1038/nphys777.

Cornilleau-Wehrlin, N., et al. (1997), The Cluster Spatio-Temporal Analysis of Field Fluctuations (STAFF) experiment, *Space Sci. Rev.*, *79*, 107–136.

Drake, J. F., M. Swisdak, H. Che, and M. A. Shay (2006a), Electron acceleration from contracting magnetic islands during reconnection, *Nature*, *443*, 553–556, doi:10.1038/nature05116.

Drake, J. F., M. Swisdak, K. M. Schoeffler, B. N. Rogers, and S. Kobayashi (2006b), Formation of secondary islands during magnetic reconnection, *Geophys. Res. Lett.*, *33*, L13105, doi:10.1029/2006GL025957.

Eastwood, J. P., et al. (2007), Multi-point observations of the Hall electromagnetic field and secondary island formation during magnetic reconnection, *J. Geophys. Res.*, *112*, A06235, doi:10.1029/2006JA012158.

Gustafsson, G., et al. (2001), First results of electric field and density observations by Cluster EFW based on initial months of operation, *Ann. Geophys.*, *19*, 1219–1240.

Haerendel, H. (1981), Magnetospheric processes possibly related to the origin of cosmic-rays, in *Origin of Cosmic Rays, IAU Symposium*, vol. 94, edited by G. Setti, G. Spada, and A. W. Wolfendale, pp. 373–391, D. Reidel, Dordrecht.

Hoshino, M., T. Mukai, T. Terasawa, and I. Shinohara (2001), Suprathermal electron acceleration in magnetic reconnection, *J. Geophys. Res.*, *106*, 25,979–25,998, doi:10.1029/2001JA900052.

Imada, S., M. Hoshino, and T. Mukai (2005), Average profiles of energetic and thermal electrons in the magnetotail reconnection regions, *Geophys. Res. Lett.*, *32*, L09101, doi:10.1029/2005GL022594.

Imada, S., R. Nakamura, P. W. Daly, M. Hoshino, W. Baumjohann, S. Mühlbachler, A. Balogh, and H. Rème (2007), Energetic electron acceleration in the downstream reconnection outflow region, *J. Geophys. Res.*, *112*, A03202, doi:10.1029/2006JA011847.

Johnstone, A. D., et al. (1997), PEACE: A plasma electron and current experiment, *Space Sci. Rev.*, *79*, 351–398.

Lin, R. P., et al. (2003), RHESSI observations of particle acceleration and energy release in an intense solar gamma-ray line flare, *Astrophys. J.*, *595*, L69–L76, doi:10.1086/378932.

Nakamura, R., et al. (2006), Dynamics of thin current sheets associated with magnetotail reconnection, *J. Geophys. Res.*, *111*, A11206, doi:10.1029/2006JA011706.

Øieroset, M., R. P. Lin, T. D. Phan, D. E. Larson, and S. D. Bale (2002), Evidence for electron acceleration up to ~300 keV in the magnetic reconnection diffusion region of Earth's magnetotail, *Phys. Rev. Lett.*, *89*(19), 195001, doi;10.1103/PhysRevLett.89.195,001.

Pedersen, A., et al. (2001), Four-point high time resolution information on electron densities by the electric field experiments (EFW) on Cluster, *Ann. Geophys.*, *19*, 1483–1489.

Pritchett, P. L. (2006a), Relativistic electron production during driven magnetic reconnection, *Geophys. Res. Lett.*, *33*, L13104, doi:10.1029/2005GL025267.

Pritchett, P. L. (2006b), Relativistic electron production during guide field magnetic reconnection, *J. Geophys. Res.*, *111*, A10212, doi:10.1029/2006JA011793.

Rème, H., et al. (2001), First multispacecraft ion measurements in and near the Earth's magnetosphere with the identical Cluster ion spectrometry (CIS) experiment, *Ann. Geophys.*, *19*, 1303–1354.

Richardson, I. G., C. J. Owen, and J. A. Slavin (1996), Energetic (>0.2 MeV) electron bursts in the deep geomagnetic tail observed by the Goddard Space Flight Center experiment on ISEE 3: Association with geomagnetic substorms, *J. Geophys. Res.*, *101*, 2723–2740.

Scholer, M. (1984), Energetic ions and electrons and their acceleration processes in the magnetotail, in *Magnetic Reconnection in Space and Laboratory Plasmas*, edited by E. W. Hones Jr., pp. 216–227, AGU, Washington, D. C.

Slavin, J. A., et al. (2003), Geotail observations of magnetic flux ropes in the plasma sheet, *J. Geophys. Res.*, *108*(A1), 1015, doi:10.1029/2002JA009557.

Sonnerup, B. U. O. (1979), Magnetic field reconnection, in *Solar System Plasma Physics*, vol. 3, pp. 45–118, Elsevier, New York.

Tanaka, K. G., I. Shinohara, and M. Fujimoto (2004), Critical thickness for two-dimensional tearing instability, *Geophys. Res. Lett.*, *31*, L03808, doi:10.1029/2003GL018955.

Wilken, B., et al. (2001), First results from the RAPID imaging energetic particle spectrometer on board Cluster, *Ann. Geophys.*, *19*, 1355–1366.

Zong, Q.-G., et al. (2004), Cluster observations of earthward flowing plasmoid in the tail, *Geophys. Res. Lett.*, *31*, L18803, doi:10.1029/2004GL020692.

M. André, Y. Khotyaintsev, and A. Vaivads, Swedish Institute of Space Physics, Box 537, SE-75121 Uppsala, Sweden.

W. Baumjohann, R. Nakamura, and A. Retinò, Space Research Institute, Austrian Academy of Sciences, Schmiedlstraße 6, A-8042 Graz, Austria. (alessandro.retino@oeaw.ac.at)

N. Cornilleau-Wehrlin, Centre d'Etude des Environnements Terrestre et Planétaires, CNRS/IPSL, 10-12 Avenue de l'Europe, F-78140 Vélizy-Villacoublay, France.

P. W. Daly and E. A. Kronberg, Max Planck Institute for Solar System Research, Max-Planck-Straße 2, D-37191 Katlenburg-Lindau, Germany.

J. P. Eastwood, Space Sciences Laboratory, University of California, 7 Gauss Way, Berkeley, CA 94720, USA.

M. Fujimoto, S. Kasahara, I. Shinohara, and K. Tanaka, Institute of Space and Astronautical Science, Japan Aerospace Exploration Agency, 3-1-1 Yoshino-dai, Sagamihara, Kanagawa 229-8510, Japan.

T. Hayakawa, Department of Earth and Planetary Sciences, Tokyo Institute of Technology, 2-12-1 Ookayama, Meguro-ku, Tokyo 152-8550, Japan.

21562202a, 2008, A12, Downloaded from https://agupubs.onlinelibrary.wiley.com/doi/10.1029/2008JA013511 by Cochrane France, Wiley Online Library on [04/06/2023]. See the Terms and Conditions (https://onlinelibrary.wiley.com/terms-and-conditions) on Wiley Online Library for rules of use; OA articles are governed by the applicable Creative Commons License